Brazilian Journal
of Chemical
Engineering

ISSN 0104-6632
Printed in Brazil
www.abeq.org.br/bjche

Vol. 32, No. 01, pp. 247 - 258, January - March, 2015
dx.doi.org/10.1590/0104-6632.20150321s00003293

AN EOS-BASED NUMERICAL SIMULATION OF THERMAL RECOVERY PROCESS USING UNSTRUCTURED MESHES

F. Marcondes[1,2*], A. Varavei[2] and K. Sepehrnoori[2]

[1]Department of Metallurgical Engineering and Material Science, Federal University of Ceará,
60.440-554, Fortaleza - CE, Brazil.
Phone: +55 (85) 3366-9355, Fax: + 55 (85) 3366-9359,
[*]E-mail: marcondes@ufc.br
[2]Petroleum and Geosystems Engineering Department, The University of Texas at Austin,
1 University Station C0300, Austin, TX, 78712-0228, USA.

(Submitted: February 12, 2014 ; Accepted: May 23, 2014)

Abstract - In the past thirty years, the development of compositional reservoir simulators using an equation of state (EOS) has been addressed in the literature. However, the development of compositional thermal simulators in conjunction with the EOS formulation, in particular, has not been addressed extensively. In this work, a fully implicit, thermal, compositional EOS-based simulator in conjunction with unstructured meshes has been developed. In this model, an equation of state is used for equilibrium calculations among phases. Also, the physical properties are calculated based on an EOS, hence obviating the need for using steam tables for calculation of water/steam properties. The governing equations for the model comprise fugacity equations, material balance, pore volume constraint and energy equation. The governing partial differential equations are solved using the EbFVM (Element based Finite Volume Method). Results for several case studies consisting of 2D and 3D reservoirs are presented in order to demonstrate the applicability of the method.
Keywords: Thermal recovery; EbFVM; EOS; Unstructured meshes.

INTRODUCTION

This paper describes the development of a fully implicit EOS thermal flooding simulator. The objective of this work is to model the thermodynamical properties and compositional effects on phase behavior calculation more accurately. In this model, all phases (oil, gas, and aqueous) are in equilibrium, and an equation of state is used for determining equilibrium between the phases. Therefore, physical properties of the phases including all water, stream and the hydrocarbon components are calculated with the EOS.

One of the most used approaches for thermal recovery in the literature is the K-value approach. In general, in a compositional reservoir simulation, phase equilibrium calculations are carried out more accurately using EOS over a wide range of pressure and temperature variations than by using the K-value approach.

The first application of EOS to calculate the phase properties was developed by Ishimoto (1985). Later on, Ishimoto *et al*. (1987) presented the results of a one-dimensional and fully implicit compositional steam-flood model. Rubin and Buchanan (1985) described a general, fully implicit, four-phase, multi-component, multidimensional formulation for steam and in-situ combustion processes. This model includes a fully implicit well model and has appropriate and robust iterative techniques for solving large thermal problems. Chein *et al*. (1989) presented a general purpose compositional simulator that included a thermal option. In this model, the user can select K-values or EOS to calculate the fluid properties. Trangenstein (1989) gave an analysis of a two-

*To whom correspondence should be addressed

component, three-phase flow thermal model. The analysis was done to study the effect of thermodynamic principles on flow equations. Brantferger *et al*. (1991) developed a simulator which has major distinctions compared to the previously mentioned formulations. They used an EOS to calculate the physical properties of each phase and water was considered as a non-ideal component and enthalpy was used as a primary variable instead of temperature.

Mifflin *et al*. (1991) introduced a fully coupled, fully implicit oil reservoir simulator. However, this formulation was implemented in a framework that supports only an IMPES and a sequential semi-implicit formulation. Fernandes *et al*. (2014) compared an IMPEC and IMPSAT approaches using Cartesian meshes in conjunction with isothermal compositional reservoir simulation. Chan and Sarioglu (1992) presented a procedure for incorporating fracture characteristics in a thermal reservoir simulator. Cicek *et al*. (1996) developed a simulator for steam injection. The simulator was based on a compositional, fully-implicit 3D multiphase, component mass and energy balance. Godderij *et al*. (1999) introduced a 3D steam drive simulator. They used an interface model, where the single-phase steam zone was separated from the two-phase liquid region by a steam condensation front. Cicek (2005) developed and tested the numerical simulation of steam displacement of oil in naturally fractured reservoirs using a fully implicit compositional formulation. He investigated the effects of capillary and gravitational forces in the matrix/fracture exchange term. Luo and Barrufet (2005), aided by their thermal simulator, studied the effect of water-in-oil solubility on oil recovery. They considered water as a pure phase, but mass transfer from water into the oil and gas phases was allowed. They performed oil/gas flash calculations in the three-phase system separately. They also had another objective function requiring water chemical potential to be same in the oil/gas flash calculation and equal to the water chemical potential in the water phase.

One key step before applying the EOS to thermal processes to handle the phase behavior calculations of water/hydrocarbon and non-hydrocarbon systems is the improvement and tuning of the EOS. Binary interaction coefficients and volume shift parameters are modified for the EOS for this kind of calculation. Bang (2005) showed good agreement between experimental data for the hydrocarbon/water and hydrocarbon/water/methanol systems at different temperatures. They modified the binary interaction coefficient and the volume shift parameter for EOS to match the experimental data. Shinta and Firoozabadi (1997) presented the binary interaction coefficients between water and hydrocarbon for EOS to handle water/hydrocarbon phase behavior calculation. Varavei and Sepehrnoori (2009) implemented and tested a 3D EOS-based thermal model with three-phase flash calculation using Cartesian grids. All the previous mentioned works are based on structured grids. Unstructured PEBI grids have been applied to the solution of a thermal recovery process (Liu *et al*., 2009; Shi *et al*., 2009). EbFVM (Element based finite volume method) has been applied to the solution of compositional and isothermal problems by Marcondes and Sepehrnoori (2007), Marcondes *et al*. (2013), and Santos *et al*. (2013). This approach is similar to the CVFEM (Control Volume Finite Element Method) approach by Forsyth (1990) and Fung *et al.* (1991), except that the approximated equations are derived from multiphase fluid flow instead of single phase flow.

In this work, we present a fully implicit, compositional EOS-based formulation in which the EOS is used for equilibrium calculation between all phases involved (oil, gas, and aqueous). The conservation equations are solved through the finite-volume in conjunction with unstructured meshes using the EbFVM method and a fully implicit approach. To the best of our knowledge, this is the first time that a complex physical model for thermal simulation is solved in conjunction with the EbFVM approach. Results for several case studies involving 2D and 3D reservoirs are presented to demonstrate the applicability of EOS-based thermal recovery in conjunction with unstructured meshes and the EbFVM approach.

PHYSICAL MODEL

Non-isothermal, multi-component, multiphase flow in a porous medium can be described by three types of equations: component material-balance equations, two phase equilibrium equations, pore volume constraint, and energy conservation equation.

The molar conservation equation for each component, assuming a full and symmetric tensor using the Einstein notation, can be written as

$$\frac{\partial(\phi N_i)}{\partial t} - \nabla\bullet\left[\sum_{j=1}^{n_p}\xi_j\, x_{ij}\,\lambda_j\overline{\overline{K}}\bullet\nabla\Phi_j\right] + R_i - \frac{\dot{q}_i}{V_b} = 0\ ;\ i = 1,2,..,n_c+1\,. \tag{1}$$

In Eq. (1), $\dot{q}_i$ represents molar rate of the point source or sink of component *i*, R_i is the reaction rate term of component *i*, V_b is the bulk volume, N_i is the number of moles of component *i* per pore volume, x_{ij} is the mole fraction of component *i* in phases *j*, ξ_j and λ_j are respectively the molar density and mobility of phase *j*, n_c is the number of hydrocarbon components, n_p is number of phases, $\overline{\overline{K}}$ is the absolute permeability tensor, ϕ is the porosity, and Φ_j is the potential of phase *j* which is given by

$$\Phi_j = P_j - \gamma_j D\,, \tag{2}$$

where P_j is the pressure of phase *j*, γ_j is the specific weight of phase *j* and *D* is the depth, which is assumed positive in the downward direction.

The energy balance equation is given by

$$\frac{\partial U^T}{\partial t} + \nabla \cdot \sum_{j=a,v,o} (\xi_j h_j \vec{v}_j) - \nabla.(\lambda_T \nabla T) = -\frac{\dot{Q}_L}{V_b} + \frac{\dot{q}_H}{V_b}\,, \tag{3}$$

where U^T is the sum of rock and total fluid internal energy per bulk volume

$$U^T = (1-\phi)\xi_r U_r + \phi \sum_{j=a,v,o} \xi_j S_j u_j\,. \tag{4}$$

In Eqs. (3) and (4), h_j is the phase molar enthalpy, λ_T is the effective conductivity coefficient, ξ_j and S_j are the phase molar density and phase saturation, ξ_r is the rock density, ϕ is the porosity, T is the temperature, $\dot{Q}_L$ is the heat loss rate through the underburden and overburden areas of the reservoir, $\dot{q}_h$ is the rate of heat injection, and the subscripts a, v, o denote the aqueous, vapor and oil phases, respectively.

The pore volume constraint, also known as the saturation constraint, is used as the independent equation. The equation for pore volume constraint is

$$\sum_{j=a,v,o} \left[\frac{N_j}{\xi_j} \right] = 1.0\,. \tag{5}$$

When the stability test reveals more than one phase, the subsequent flash calculation determines the mole ratios and the compositions of the phases. There are two different methods of flash calculation in the approach investigated in this work: the accelerated successive substitution method by Mehra *et al*. (1983) and minimization of the Gibbs free energy using the method presented by Trangenstein (1987), which is an implementation of the reduced gradient approach (Perschke, 1988). In this work, these two methods are combined to speed-up the convergence rate. First, the accelerated successive substitution method is used to provide a reasonable initial estimate, and then we switch to the Gibbs free energy method in order to accelerate the convergence. In this work, we use the EOS proposed by Peng and Robinson (1976) to evaluate the physical properties and conduct the phase stability test. The following equations are solved to calculate the phase ratios:

$$g_j(L_2 \ldots L_{n_p}) = \sum_{i=1}^{n_c} \frac{z_i(K_{ij}-1)}{1 + \sum_{j=2}^{n_p} L_j(K_{ij}-1)}\,, \tag{6}$$

$$L_1 = 1 - \sum_{j=2}^{n_p} L_j\,. \tag{7}$$

Phase mole fractions of the reference phase (phase 2) are calculated as follows:

$$x_{i2} = \frac{z_i}{1 + \sum_{j=2}^{n_p} L_j(K_{ij}-1)}\,,\ i = 1,\ldots,n_c\,. \tag{8}$$

The mole fractions of the other phases are calculated as follows:

$$x_{ij} = \frac{z_i K_{ij}}{1 + \sum_{j=2}^{n_p} L_j(K_{ij}-1)}\,,\ i = 1,\ldots,n_c, j = 2,\ldots,n_p\,. \tag{9}$$

In Eqs. (6) through (9), z_i denotes the overall composition of component *i*, K_{ij} is the equilibrium ratio of component *i* in phase *j*, L_j is the ratio of moles in phase *j* to the total number of moles in the mixture. Two equilibrium equations are needed to show a maximum of three phases at equilibrium in each gridblock. In the initialization step, after the stability test, the flash calculation is performed to calculate mole ratios of the phases, the composition of the phases, the phase saturation, and the initial amount of the phases in place. Next, the equilibrium equations are solved along with other governing

equations. Equilibrium equations for all the components, considering the oil phase as the reference phase, are given by

$$f_{i,gas} - f_{i,oil} = lnK_{1,i} + ln\varphi_{i,g} - ln\varphi_{i,oil} = 0, \quad i = 1,...,n \tag{10}$$

$$f_{i,L} - f_{i,oil} = lnK_{2,i} + ln\varphi_{i,L} - ln\varphi_{i,oil} = 0, \quad i = 1,...,n \tag{11}$$

In these above equations, $f_{i,j}$ is fugacity of component i in phase j, $\varphi_{i,j}$ is the fugacity coefficient of component i in phase j, and the subscript L denotes the second liquid phase. In Eqs. (10) and (11), n denotes the total number of hydrocarbon components plus the water component. Subsequent to the calculation of the Z-factor from EOS, the molar density is calculated by

$$\xi_j = \frac{P_j}{Z_j RT}. \tag{12}$$

In Eq. (12), Z_j and P_j are the compressibility factor and pressure of phase j, respectively, and R is the universal gas constant. The fugacity coefficient, enthalpy (h_j), and internal energy (u_j) of phase j are calculated from the EOS as follows:

$$ln\varphi_{ij} = \frac{b_i}{b_m}\left(Z_j - 1\right) - ln\left(Z_j - B_j\right) - \frac{A_j}{2\sqrt{2}B_j}\left(\frac{2}{a_j}\sum_{m=1}^{n_c} x_{mj}a_{im} - \frac{b_i}{b_m}\right) ln\left[\frac{Z_j + \left(1+\sqrt{2}\right)B_j}{Z_j + \left(1-\sqrt{2}\right)B_j}\right], \tag{13}$$

$$h_j = \frac{T\dfrac{\partial a_{m,j}}{\partial T} - a_{m,j}}{b_{m,j}} ln\left(\frac{Z_j + (\sqrt{2}+1)B_j}{Z_j + (\sqrt{2}-1)B_j}\right) + RT(Z_j - 1) + h_j^{\circ}, \tag{14}$$

$$h_j^{\circ} = \sum_{i=1}^{n_c} x_{ij} h_i^{\circ}, \tag{15}$$

$$h_i^{\circ} = Cp_{1,i}^{\circ}(T - T_{ref}) + \frac{Cp_{2,i}^{\circ}}{2}(T^2 - T_{ref}{}^2) + \frac{Cp_{3,i}^{\circ}}{3}(T^3 - T_{ref}{}^3) + \frac{Cp_{4,i}^{\circ}}{4}(T^4 - T_{ref}{}^4), \tag{16}$$

$$u_j = h_j - P_j v_j. \tag{17}$$

The parameters h_j° and h_i° are the reference enthalpies for the phase j and component i, $a_{m,j}$, $b_{m,j}$, B_j are parameters of the equation of state, and v_j is the molar volume of phase j. The reference state (ref) is the ideal gas for the particular component; the coefficients $Cp_{1,i}^{\circ} \ldots Cp_{4,i}^{\circ}$ are the heat capacity coefficient for component i in the ideal gas condition considered as the reference state. Viscosities of the hydrocarbon phases are evaluated through the Lohrenz's correlation (Lohrenz *et al*., 1964).

The heat-loss from overburden and underburden is calculated by the Vinsome and Westerveld (1980) method, which assumes a temperature profile in the form of:

$$T(t,z) = (\theta - \theta^0 + b_1 z + b_2 z^2)\exp(-z/d) + \theta^0, \tag{18}$$

where $T(t,z)$ is overburden/underburden temperature at time t at a distance of z from the reservoir surface; the interface between the reservoir and cap and base rock is defined to be at $z=0$. b_1 and b_2 are time-dependent parameters, θ is the temperature difference with respect to the surrounding initial temperature and d is a diffusion length, defined by $d = \frac{1}{2}\sqrt{\eta t}$, where η is the thermal diffusivity $\eta = \frac{\lambda_r}{c_r \xi_r}$ and λ_r is the thermal conductivity of the rock, and c_r is the rock heat capacity. The parameters b_1 and b_2 are obtained by the equations given by Vinsome and Westerveld (1980):

$$b_1^{n+1} = \frac{\dfrac{\eta\Delta t(\theta^{n+1} - \theta^0)}{d^{n+1}} + \tau^n - \dfrac{(d^{n+1})^3(\theta^{n+1} - \theta^n)}{\eta\Delta t}}{3(d^{n+1})^2 + \eta\Delta t}, \tag{19}$$

$$b_2^{n+1} = \frac{2b_1^{n+1}(d^{n+1}) - (\theta^{n+1} - \theta^0) + \dfrac{(d^{n+1})^2(\theta^{n+1} - \theta^n)}{\eta\Delta t}}{2(d^{n+1})^2} \tag{20}$$

$$\tau^n = \left[\left(\theta - \theta^0\right)d + b_1 d^2 + 2b_2 d^3\right]^n, \tag{21}$$

$$\dot{Q}_{loss} = \lambda_r A \left[\frac{(\theta^{n+1} - \theta^0)}{d^{n+1}} - b_1^{n+1} \right], \quad (22)$$

where A is the cross-sectional area for heat-loss to overburden and underburden areas.

The viscosity of the hydrocarbon phases is determined by Lohrenz's correlation (Lohrenz *et al*., 1964); for the aqueous phase the Grabowski function (Grabowski *et al*., 1979) is used. Tables of phase viscosities as a function of temperature can also be used.

NUMERICAL APPROACH

In this work, the EbFVM described by Marcondes and Sepehrnoori (2010), Marcondes *et al*. (2013), and Santos *et al*. (2013) was used to solve the 2D and 3D unstructured reservoirs, respectively. In the EbFVM approach we borrow from the finite-element method the idea of elements and shape functions. Then, each element is divided into sub-elements and the conservative equations are integrated for each sub-element. After the division, we call each sub-element of sub-control volume because the conservative equations are integrated for each one of these sub-elements. For a 2D discretization, the reservoir can be discretized using triangles, quadrilaterals, or a mix of these two elements. For 3D discretization, the grid can be composed of hexahedrons, tetrahedrons, prisms, or pyramids. In general, prisms and pyramids are used as transitional elements when hexahedrons and tetrahedrons are combined. Figure 1 presents the four elements employed for the 3D discretization.

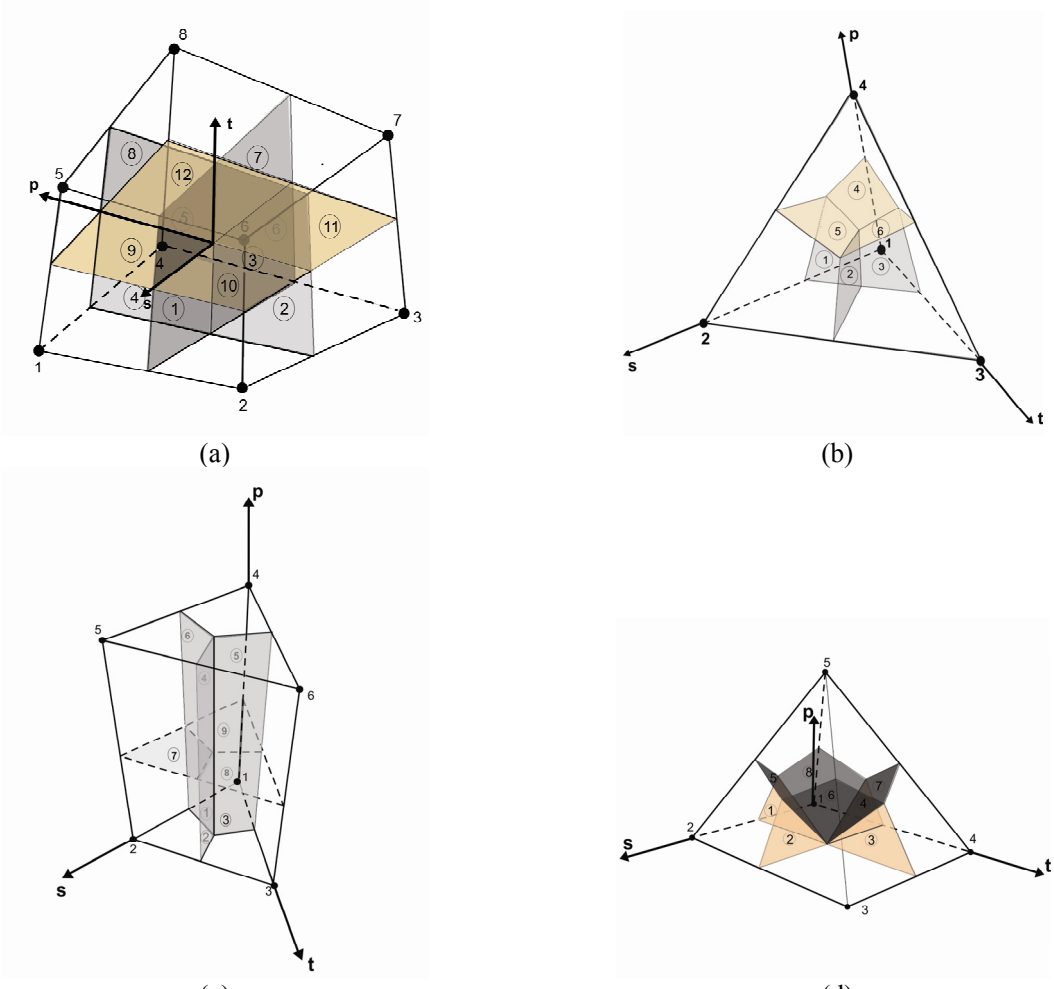

(a) (b) (c) (d)

Figure 1: Elements employed for the 3D discretization and their respective sub-control volumes: (a) hexahedron, (b) tetrahedron, (c) prism, and (d) pyramid.

According to the number of vertices, each element is divided into sub-elements and the conservative equations are integrated over each one of these sub-elements. The approximate equation for each control volume that surrounds each vertex of the mesh is obtained from the summation of all the sub-elements that share that vertex. The integration procedure is performed for the conservative equations (molar material balance and the energy equations). In order to present details of the numerical approach, we integrate the energy equation, Eq. (3), in time and for each one of the sub-control volumes. Performing an integration in time and for each one of the sub-control volumes and applying the Gauss theorem for the advective and diffusive fluxes the following equation is obtained:

$$\int_{V,t} \frac{\partial U^T}{\partial t} dV dt + \int_{A,t} \sum_{j=a,v,o} \xi_j h_j \vec{v}_j . d\vec{A} dt - \int_{A,t} \lambda_T \nabla T \, d\vec{A} dt = - \int_{V,t} \left(\frac{\dot{Q}_L}{V_b} + \frac{\dot{q}_H}{V_b} \right) dV dt \quad , \tag{23}$$

where dV and $d\vec{A}$ denote, respectively, the volume of each sub-control and the area of each integration surface. In Fig. 1, the numbers that reside inside a circle refer to the integration surfaces and the others refer to the vertices. Considering for instance, the pyramid element and the vertex 2, V is the volume of the region limited by the base and lateral surfaces (2-3-5-2 and 2-6-5-2) and the integration surfaces 2, 5, 1 and $d\vec{A}$ denote the areas of the integration surfaces 1, 2, and 5. In order to evaluate the accumulative term and advective and diffusive fluxes, it is necessary to define the shape functions. The shape functions for triangular and quadrangular elements are respectively given by:

$$N_1(s,t) = 1 - s - t \; ; \; N_2(s,t) = s \; ; \; N_3(s,t) = t \, , \tag{24}$$

$$N_1(s,t) = \frac{1}{4}(1-s)(1-t) \; ; \; N_2(s,t) = \frac{1}{4}(1+s)(1-t); \quad N_3(s,t) = \frac{1}{4}(1+s)(1+t) \; ; \; N_4(s,t) = \frac{1}{4}(1-s)(1+t), \tag{25}$$

where s and t denote the local axes in the transformed plane. For a triangular element, s and t vary from 0 to 1, while for the quadrilateral element s and t vary from -1 to 1. The shape functions for hexahedron, tetrahedron, prism and pyramid elements are respectively given by:

$$N_1(s,t,p) = \frac{(1+s)*(1-t)*(1+p)}{8} \; ; \quad N_2(s,t,p) = \frac{(1+s)*(1-t)*(1-p)}{8} \quad N_3(s,t,p) = \frac{(1-s)*(1-t)*(1-p)}{8} \; ; \quad N_4(s,t,p) = \frac{(1-s)*(1-t)*(1+p)}{8} \quad N_5(s,t,p) = \frac{(1+s)*(1+t)*(1+p)}{8} \; ; \quad N_6(s,t,p) = \frac{(1+s)*(1+t)*(1-p)}{8} \quad N_7(s,t,p) = \frac{(1-s)*(1+t)*(1-p)}{8} \; ; \quad N_8(s,t,p) = \frac{(1-s)*(1+t)*(1+p)}{8} \tag{26}$$

$$N_1(s,t,p) = 1 - s - t - p \; ; \; N_2(s,t,p) = s \quad N_3(s,t,p) = t \; ; \; N_4(s,t,p) = p \tag{27}$$

$$N_1(s,t,p) = (1-s-t)*(1-p); \quad N_2(s,t,p) = s*(1-p) \; ; \; N_3(s,t,p) = t*(1-p); \quad N_4(s,t,p) = p*(1-s-t) \; ; \; N_5(s,t,p) = s*p; \quad N_6(s,t,p) = t*p \tag{28}$$

$$N_1(s,t,p) = \frac{1}{4}[(1-s)(1-t) - p + s*t*p/(1-p)] \quad N_2(s,t,p) = \frac{1}{4}[(1+s)(1-t) - p - s*t*p/(1-p)] \quad N_3(s,t,p) = \frac{1}{4}[(1+s)(1+t) - p - s*t*p/(1-p)] \quad N_4(s,t,p) = [(1-s)(1+t) - p - s*t*p/(1-p)] \quad N_5(s,t,p) = p \tag{29}$$

The s, t, and p that appear in the shape functions denote the local axis in the transformed plane. For the hexahedron element each of these axes varies from -1 to 1. For the other elements the variation is from 0 to 1. In order to obtain the shape functions for the hexahedron element, we assumed a tri-linear variation of the physical properties with x, y, and z. Using the shape functions, we can evaluate the gradients, areas and volumes that are necessary to finalize the integration of Eq. (22). The discretized equations are then linearized through a Newton method and solved together with the molar balance equations. Further details of the numerical approach employed in this paper can be found in Marcondes

and Sepehrnoori (2010), Marcondes *et al*. (2013), and Santos *et al*. (2013).

TEST PROBLEMS

This section presents four simulation case studies using the EbFVM approach and the finite-volume method in conjunction with Cartesian meshes. The first two case studies were used to validate the present formulation with Cartesian meshes. The current implementation of the GPAS simulator has been validated and compared with available analytical solutions from the literature (Varavei and Sepehrnoori, 2009). Case 1 is the simulation of two-component injection in a 2D quarter-of-five spot. Figure 2 presents the two-grid configurations used for Case 1, and Table 1 shows the fluid and physical properties used. All four case studies used the same Corey's relative permeability data given in Table 2. Case 2 again refers to a quarter-of-five-spot, but now the 3D variation was allowed and we considered four components instead of two. The components considered for the rest of the cases investigated in the present paper were the following: C_{10}, C_{15}, C_{20}, water. The initial overall fluid compositions inside the reservoir were the following: 0.0004, 0.0006, 0.199, 0.8; and the injected fluid compositions were the following: 0.0, 0.0, 0.0, 1.0. Except for Case 3, which is a 3D heterogeneous quarter-of-five-spot, the permeability in the z-direction is equal to the x and y-directions presented in Table 1. For Cases 2 through 4, the bottom hole pressure for the producer wells is equal to 4 MPa (580 psi). Figure 3 presents the porosity and permeability field for the x-direction used for Case 3. The same permeability value is used for the y-direction; one tenth of the value of the x-direction is chosen for the z-direction. Case 4 refers to simulating of an irregular reservoir. Figure 4 presents the two refined meshes employed (a hexahedron and a hybrid). The top and bottom views of the configuration are presented in Fig. 4. For this case, the rate for the injecting well was set to half of the injection rate of the one presented in Table 1.

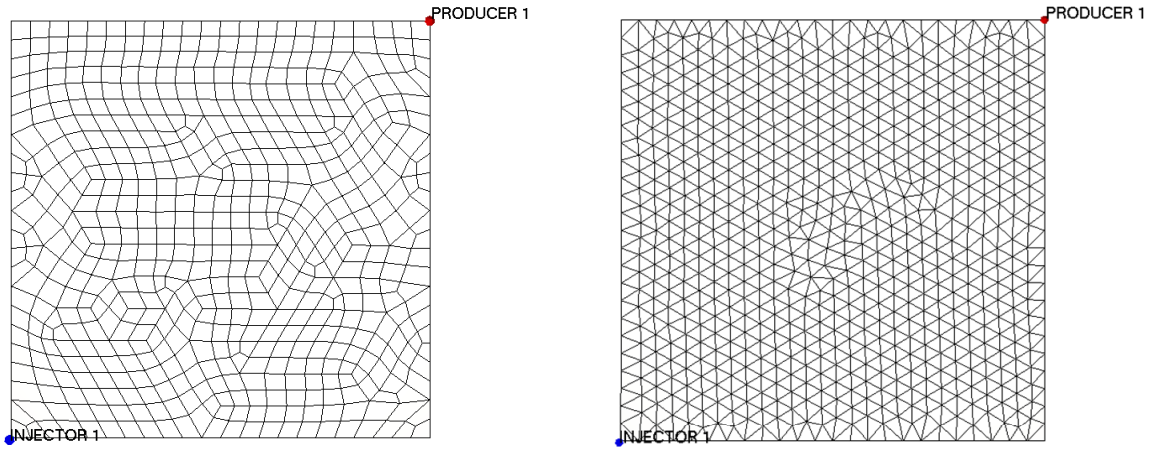

(a) (b)

Figure 2: Grid configurations – case 1. (a) Quadrilateral grid – 619 vertices, (b) Triangular grid – 710 vertices.

Table 1: Input data for Case 1.

Reservoir data	Initial conditions	Physical properties and well conditions
Reservoir dimension ($L_x = L_y$ = 170.688 m, L_z = 30.48 m)	Reservoir pressure = 4.137 MPa (600 psi)	Bottom hole pressure for the producer well = 4.137 MPa (600psi)
Absolute permeability ($K_{xx} = K_{yy}$) = 2.467×10^{-13} m^2 (250 mD)	Reservoir temperature = 60.18 ^oC (600 ^oR)	Injected well rate = 271.443 m^3/day (2,276.435 barrels/day)
Porosity = 0.3	Overall fraction of components (C_{17}, water) = 0.3, 0.7	Injected temperature = 126.85 ^oC (720 R)
Rock heat capacity = $2,345743 \times 10^6$ J/(m^3.^{o}C) (35 BTU/(ft^3.^{o}R))		Injected mole fraction (C_{17}, water) =0.0, 1.0
Reservoir thermal conductivity = 2.524 W/(m.^{o}C) (35 BTU/(ft.day.^{o}R))		
Caprock thermal conductivity = 1.80 W/(m.^{o}C) (25 BTU/(ft.day.^{o}R))		

Table 2: Corey's model relative permeability data.

	Aqueous	Oil	Gas
End point relative permeability	0.5	0.7	0.8
Residual saturation	0.1	0.2	0.06
Exponent of relative permeability	2.5	2.0	1.5

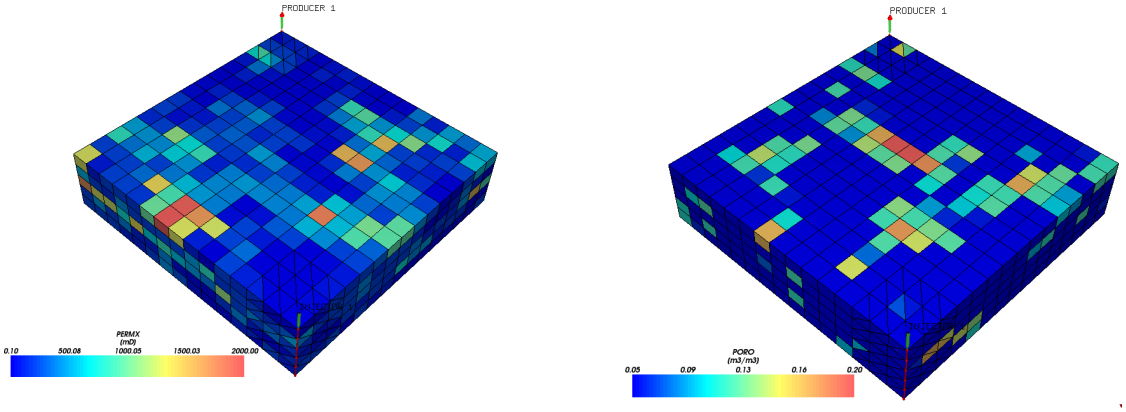

(a) (b)

Figure 3: Absolute permeability in the x-direction and porosity for Case 3.

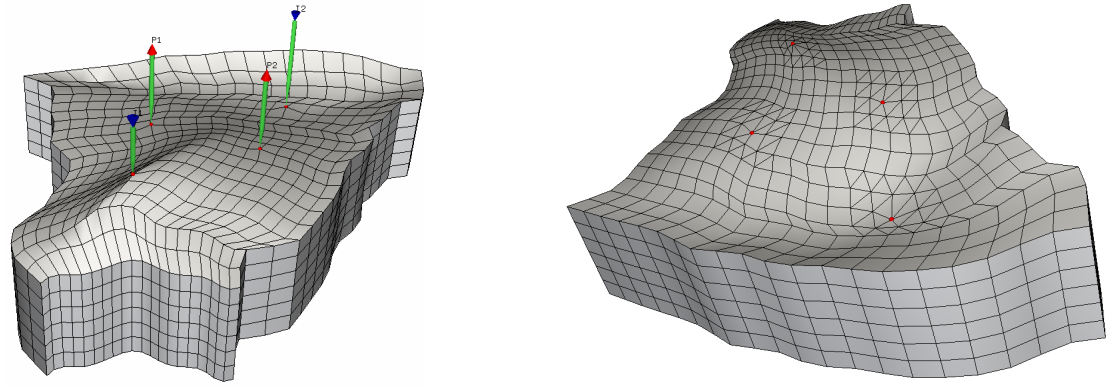

(a) (b)

Figure 4: Grid configurations used for Case 4: (a) hexahedron grid (3087 vertices, 2400 elements) and (b) hybrid grid (3475 vertices, 3086 tetrahedrons, 1632 hexahedrons, 1925 pyramids).

RESULTS

Figure 5 presents the results in terms of oil and aqueous phase rates at standard surface conditions for Case 1 using two refined unstructured meshes: quadrilateral and triangular elements. The results obtained with a refined Cartesian mesh are also shown. From this figure, it is possible to verify that the results obtained with the unstructured meshes are in good agreement with those obtained with the Cartesian mesh. We also infer that the Cartesian mesh was as accurate as the unstructured meshes employed. It is important to mention that the difference in phase density between oil and aqueous phase is not large and therefore the grid orientation effect is small. For such cases, it is expected that the Cartesian mesh will present good results, since it is very uniform along the reservoir.

Figure 6 presents the results in terms of oil and aqueous phase volumetric rates at standard surface conditions for Case 2, that is, again a uniform case, but the 3D variation is now taken into account and 4 components are considered. The hybrid mesh is composed of 975 hexahedrons, 660 tetrahedrons, and 300 pyramidal elements. Although small differences in the breakthrough were observed, especially for the hybrid mesh, the results obtained from all unstructured and the Cartesian meshes are in good agreement. It is important to mention that all element types for the 3D discretization at this point have been evaluated.

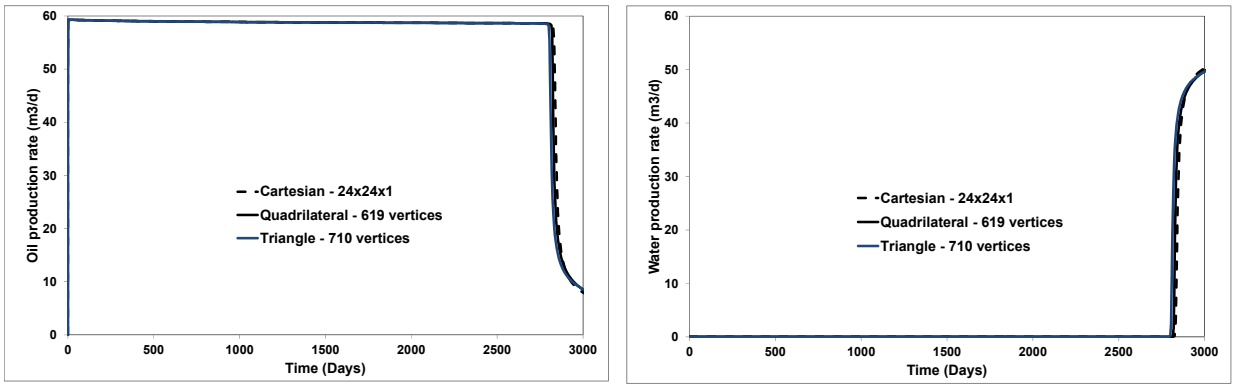

(a) (b)

Figure 5: Results for Case 1. (a) Oil production rate vs. time (b) Water production rate vs. time

Figure 7 presents the results in terms of oil and aqueous phase volumetric rates at standard surface conditions for Case 3 (heterogeneous case). The main difference between the results shown in Figure 6 is in the breakthrough time, which in this case happens early and is caused by the increase of absolute permeability in some areas of the reservoir compared to the homogeneous case (Case 2). The aqueous phase saturation at four simulation times in conjunction with the hybrid mesh is shown in Figure 8. Due to the heterogeneities in porosity and permeability the saturation shown in Fig. 8 is completely asymmetrical.

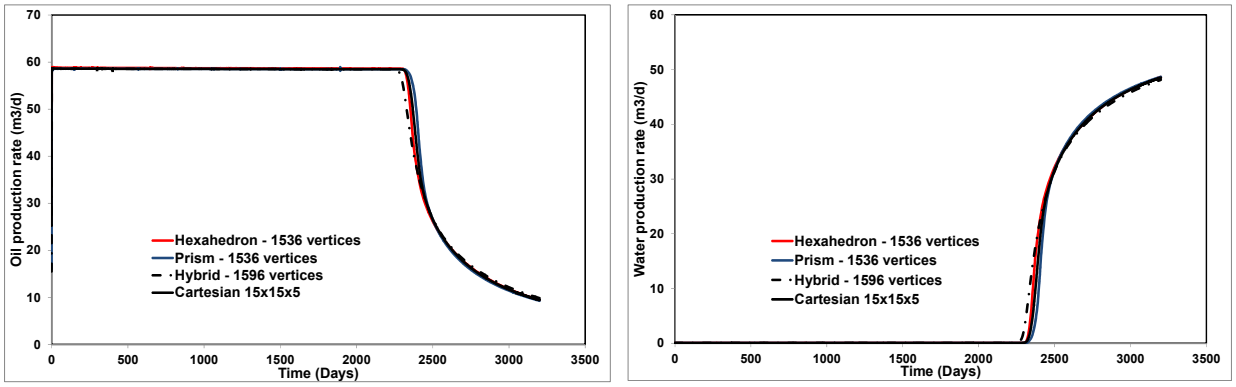

(a) (b)

Figure 6: Results for Case 2. (a) Oil production rate vs. time (b) Water production rate vs. time.

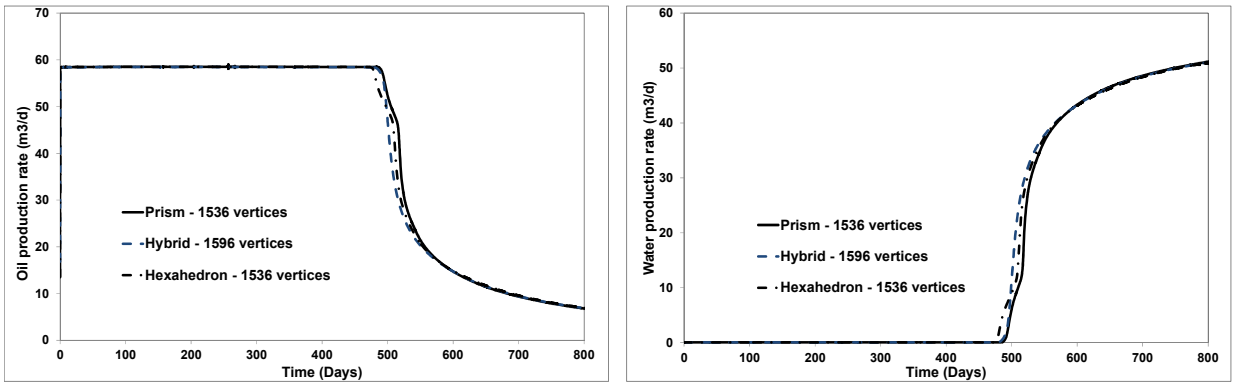

(a) (b)

Figure 7: Results for Case 3. (a) Oil production rate vs. time (b) Water production rate vs. time.

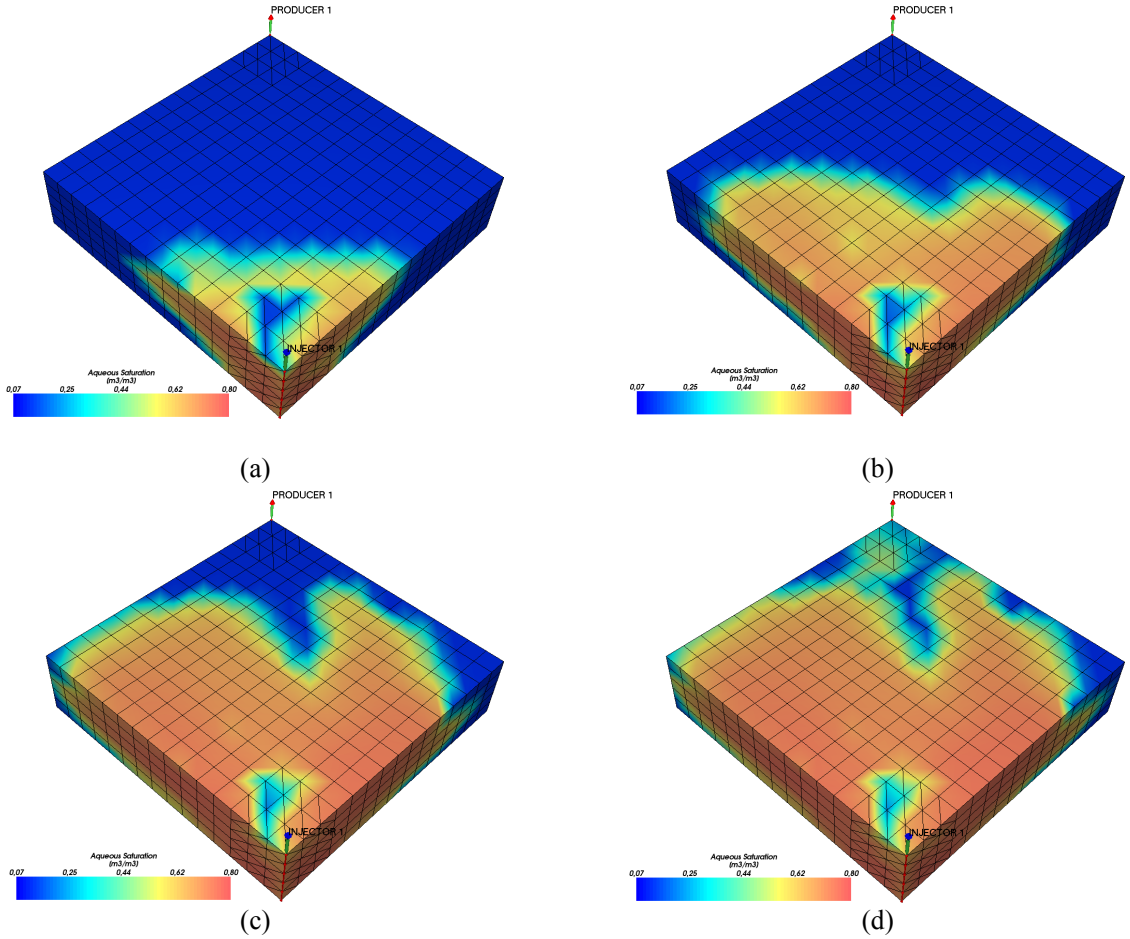

Figure 8: Aqueous phase saturation – hybrid grid: (a) 80 days, (b) 200 days, (c) 400 days, (d) 500 days.

The results for the last case study, in terms of volumetric rates of oil and aqueous phase at standard surface conditions, are shown in Figure 9. Although the two grid configurations investigated are completely different, the results in terms of volumetric rates are in good agreement. Figure 10 shows the aqueous phase saturations at two simulated times in conjunction with the hybrid mesh.

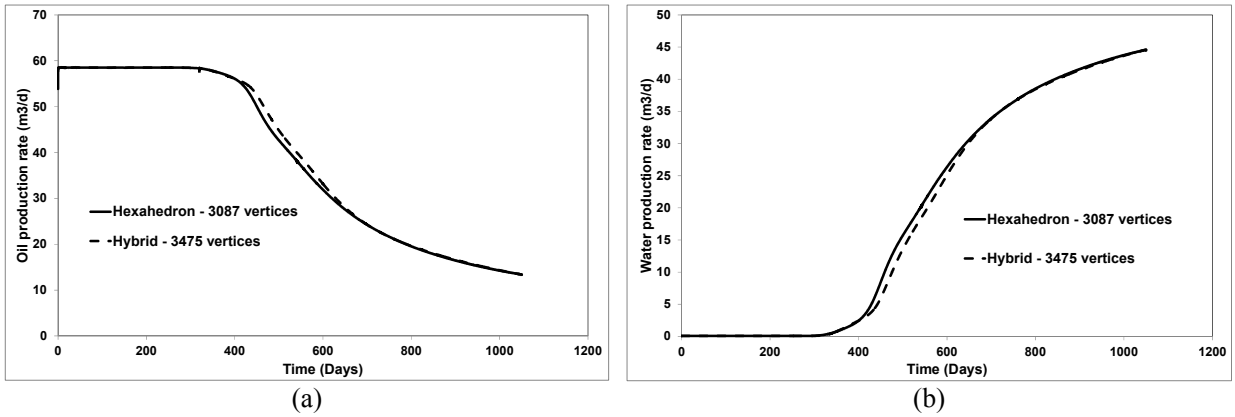

Figure 9: Results for Case 4. (a) Oil production rate vs. time (b) Water production rate vs. time.

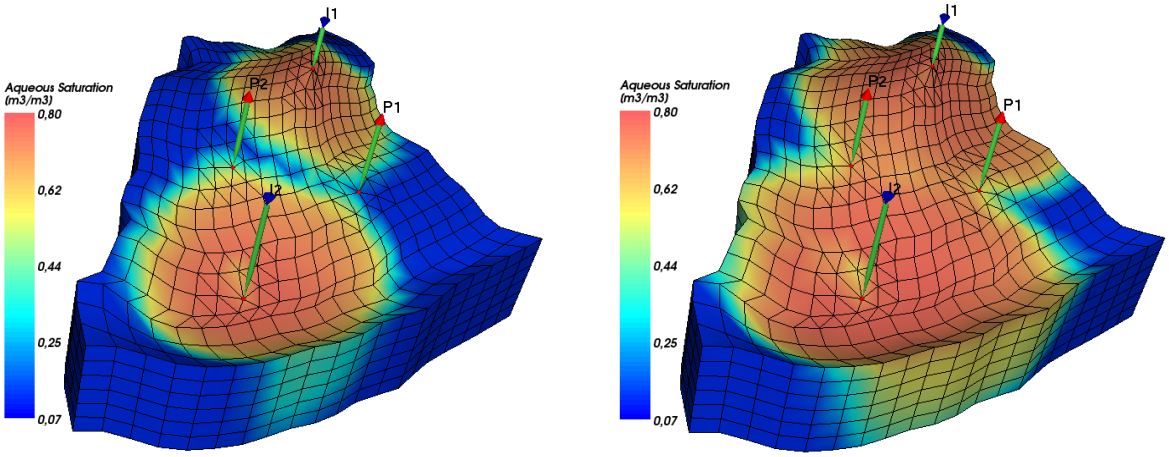

(a) (b)

Figure 10: Aqueous phase saturation – hybrid grid: (a) 400 days, (b) 1,000 days.

CONCLUSIONS

In this paper, we presented an EOS-based thermal simulation in conjunction with the finite-volume method using unstructured meshes. An equation of state is used for equilibrium calculations between all phases (oil, gas, and aqueous). Also, the physical properties are calculated based on an EOS, hence obviating the need for using steam tables for calculation of water/steam properties. A fully implicit procedure is used to solve the approximate equations arising from the discretization procedure. From the several cases investigated, it is observed that, due mainly to small differences in the injected (aqueous) and the resident oil, the grid orientation is not large. Henceforth, the results obtained with the Cartesian meshes are in good agreement with the ones obtained with unstructured meshes. However, the approach using unstructured meshes implemented and tested in the present paper has several advantages compared to Cartesian meshes because it allows an easy modeling of irregular shapes, deviated wells, discrete fractures and sealing faults and, therefore, it is an attractive approach to overcome most of problems confronted with the Cartesian meshes commonly used in petroleum reservoir simulators.

ACKNOWLEDGMENTS

This work was conducted with the support of the Reservoir Simulation Joint Industry Project, a consortium of operating and service companies at the Center for Petroleum and Geosystems Engineering at The University of Texas at Austin. Also, the second author would like to thank CNPq (The National Council for Scientific and Technological Development of Brazil) for their financial support through the grant No. 305415/2012-3. We like to thank Dr. Chowdhury K. Mamum for his comments on this manuscript. We also like to thank the ESSS Company for giving us the license of the Kraken reservoir simulation post-processor for performing the pre- and post-processing of the results.

REFERENCES

Bang, V., Phase behavior study of hydrocarbon-water-alcohol mixture. MS. Thesis, The University of Texas at Austin (2005).

Brantferger, K. M., Pope, G. A. and Sepehrnoori, K., Development of a thermodynamically consistent, fully implicit, compositional, equation-of-state, steamflood simulator. SPE Symposium on Reservoir Simulation, Anaheim, California, USA, February 17-20 (1991).

Cicek, O. and Ertekin, T., Development and testing of a new 3-D field scale fully implicit multi-phase compositional steam injection simulator. European 3-D Reservoir Modelling Conference, Stavanger, Norway, April 16-17 (1996).

Cicek, O., Numerical simulation of steam displacement of oil in naturally fractured reservoirs using fully implicit compositional formulation: A comparative analysis of the effects of capillary and gravitational forces in matrix/fracture exchange term. SPE Annual Technical Conference and Exhibition, Dallas, Texas, USA, October 9-12 (2005).

Chan, M. Y. S. and Sarioglu, G., Numerical modeling

of cyclically steamed and fractured oil-sand reservoirs. International Meeting on Petroleum Engineering, Beijing, China, March 24-27 (1992).

Chein, M. C. H., Yardumain, H. E., Chung, E. Y. and Todd, W. W., The formulation of a thermal simulation model in a vectorized, general purpose reservoir simulator. 10th SPE Symposium on Reservoir Simulation, Houston, Texas, USA, February 6-8 (1989).

Fernandes, B. R. B., Varavei, A., Marcondes, F. and Sepehrnoori, K., Comparison of an IMPEC and a semi-implicit formulation for compositional reservoir simulation. Braz. J. Chem. Eng., 31(4), 977-991 (2014).

Forsyth, P. A., A control-volume, finite-element method for local mesh refinement in thermal reservoir simulation. SPE Reservoir Engineering, 5(4), 561-566 (1990).

Fung, L. S., Hiebert, A. D. and Nghiem, L., Reservoir simulation with a control-volume finite-element method. 11th SPE Symposium on Reservoir Simulation, Anaheim, California, USA, February (1991).

Godderij, R. R., Bruining, J. and Molenaar, J., A fast 3D interface simulator for steamdrives. SPE Journal, 4(4), 400-408 (1999).

Grabowski, J. W., Vinsome, P. K., Lin, R. C., Behie, A. and Rubin, B., A fully implicit general purpose finite difference thermal model for in situ combustion and steam. Annual Meeting of the Society of Petroleum Engineering of AIME, Las Vegas, Nevada, USA, September 23-26 (1979).

Ishimoto, K., One–dimensional fully implicit compositional model for steam flooding. MS Thesis, University of Texas at Austin (1985).

Ishimoto, K., Pope, G. A. and Sepehrnoori, K., An equation of state steam simulator. *In situ*, 11(1), 1-37 (1987).

Lohrenz, J., Bray, B. G. and Clark, C. R., Calculation viscosities of reservoir fluids from their compositions. Trans., AIME, 142, 159-172 (1964).

Liu, K., Subramanian, G., Dratler, D. I., Lebel, J. P. and Yerian, J. A., A general unstructured-grid, equation-of-state-based, fully implicit thermal simulator for complex reservoir processes. SPE Journal, 14(2), 338-354 (2009).

Luo, S. and Barrufet, M. A., Reservoir-simulation study of water-in-oil solubility effect on oil recovery in the steam-injection process. SPE Reservoir Evaluating & Engineering, 8(6), 528-533 (2005).

Marcondes, F., Santos, L. O. S., Varavei, A. and Sepehrnoori, K., A 3D hybrid element-based finite-volume method for heterogeneous and anisotropic compositional reservoir simulation. Journal of Petroleum Science and Engineering, 108, 342-351 (2013).

Marcondes, F. and Sepehrnoori, K., An element-based finite-volume method approach for heterogeneous and anisotropic compositional reservoir simulation. Journal of Petroleum Science and Engineering, 73(12), 99-106 (2010).

Mehra, R. K., Heidemann, R. A. and Aziz, K., An accelerated successive substitution algorithm. Can. J. Chem. Eng, 61, 590-596 (1983).

Mifflin, R. T., Watts, J. W. and Weiser, A., A fully coupled, fully implicit reservoir simulator for thermal and other complex reservoir processes. SPE Symposium on Reservoir Simulation, Anaheim, California, USA, February 17-20 (1991).

Peng, D. Y. and Robinson, D. B. A., A new two-constant equation of state. Industry and Engineering Chemistry: Fundamentals, 15, 59-64 (1976).

Perschke, D. R., Equation of state behavior modeling for compositional simulator. Ph.D. Dissertation, The University of Texas at Austin (1988).

Rubin, B. and Buchanan, W. L., A general purpose thermal model. SPE Journal, 15(2), 202-214 (1985).

Santos, L. O. S., Marcondes, F. and Sepehrnoori, K., A 3D compositional miscible gas flooding simulator with dispersion using element-based finite-volume method. Journal of Petroleum Science and Engineering, 112, 61-68 (2013).

Shi, X., Chang, Yih-Bor Obi, E. and Lim, Kok-Thye, A general unstructured grid, parallel, thermal simulator and its application for large scale thermal models. SPE Reservoir Simulation Symposium, The Woodlands, Texas, USA, February 2-4 (2009).

Shinta, A. A. and Firoozabadi, A., Prediction phase behavior of water/reservoir crude systems with the association concept. SPE Reservoir Engineering, 12(2), 131-137, May (1997).

Trangestein, J. A., Customized minimization techniques for phase equilibrium computation in reservoir simulation. Chem. Eng. Sc., 42, 2847-2863 (1987).

Trangenstein, J. A., Analysis of a model and sequential numerical method for thermal reservoir simulation. European Conference on the Mathematics of Oil Recovery, Cambridge, England, July 25-27 (1989).

Vinsome, P. K. W. and Westerveld, J., A simple method for predicting cap and base rock heat losses in thermal reservoir simulators. J. Can. Pet. Tech., 19(3), 87-90 (1980).

Varavei, A. and Sepehrnoori, K., An EOS-based compositional thermal reservoir simulator. SPE Reservoir Simulation Symposium, Woodland, Texas, USA, February 2-4 (2009).